Research Article

Thermal Analysis and Structural Optimization of High-Efficiency Fuel Submersible Hot Water Machine

Zhaozhe Zhu (ID), **Youmin Wang** (ID)**, and Yingshuai Zhang** (ID)

School of Mechanical and Automotive Engineering, Anhui Polytechnic University, Wuhu, Anhui 241000, China

Correspondence should be addressed to Zhaozhe Zhu; 2190130110@stu.ahpu.edu.cn

Based on the oil quality of diesel oil, the thermal efficiency and fuel consumption of the fuel-burning submersible hot water machine were calculated. The structure of the fuel-burning submersible hot water machine was designed. The heat transfer calculation of the flame tube and convection surface of the high-efficiency fuel submersible hot water machine was carried out, and the overall heat balance of the system was checked. ANSYS was used to analyze and study the mechanical and thermodynamic properties of the fuel-based submersible hot water machine, and the simulation results were compared with the theoretical calculation results. The thermal field of the flame tube and the threaded tube was simulated, and the influence of the temperature field on the flame tube was analyzed. The changes in the total deformation and strength of the flame tube under the thermal structure coupling were studied. The thermal efficiency of oil-fired submersible hot water machine was studied, and the relevant factors affecting the thermal efficiency of oil-fired submersible hot water machine were put forward. The main factors affecting thermal efficiency were analyzed and mathematically modeled. The air supply model and the convective heat transfer model of the threaded tube were established. The main parameters that affected the thermal efficiency of the threaded tube were optimized. In the end, the design scheme of a high-efficiency fuel-type submersible hot water machine was obtained.

1. Introduction

Hot water machines have been widely used in various fields, especially in areas where the demand for hot water is relatively large. There are many types of hot water machines, and the application types of hot water machines are also different in different working locations and environments. For example, in residential areas, the residents use gas-fired hot water machines; in school bathrooms, electric heating hot water machines are often used; in some areas abroad, hot water machines using geothermal energy have appeared [1, 2]. In some engineering fields, such as the diving industry, electric-heated diving hot water machines have appeared. Researchers at home and abroad have done some research studies on different types of hot water machines to varying degrees. However, there has been a lot of research on related water boiler [3–5]. But there are very few research studies on oil-fired submersible hot water machines at home and abroad. Johnson and Beausoleil-Morrison [6] designed a

model for the performance prediction of gas tankless water heaters and calibrated and verified the model, but they did not study and optimize the mechanical properties of the water heater structure, nor did they conduct in-depth thermal research on the hot water machine. Lenhard and Malcho [7] established a mathematical model for heating hot water by an indirect heating water heater and made a CFD simulation of the established mathematical model. Based on the simulation results, the parameters of the indirect heating hot water machine were optimized. But they did not research and optimize the structure and mechanical properties of indirect heating hot water machines. Liu et al. [8] proposed a high-throughput screening method (HTS) based on machine learning to design and screen the best combination of external characteristics of water-in-glass evacuated tube solar water heaters (WGET-SWHs) with high heat collection rate, but there is no research on the relationship between the structure and heat of the hot water machines. This paper not only researches and optimizes the structure and mechanical

performance of the hot water machine, but also conducts in-depth thermal research on the hot water machine and optimizes the thermal efficiency of the submersible hot water machine by establishing a mathematical model.

2. Analysis and Calculation of Original Data and Fuel Characteristics of Oil-Fired Submersible Hot Water Machine

2.1. The Original Data of the Fuel-Type Diving Hot Water Machine. This article comes from a diving equipment factory. According to the actual needs of the project and the previous experience in the development of electric-heated submersible hot water machines, the author finally plans to develop an oil-fired submersible hot water machine with 0# diesel as fuel. The original data of the fuel oil type submersible water heater to be developed by a diving equipment factory are as follows: the fuel is 0# diesel, the input liquid is seawater and fresh water, the water input pressure is 3.4–10 bar, the input flow is at least 45 L/min, the output pressure is the highest 68 bar, and the output flow is about 38 L/min. The volume of the water heater is about 250 L, the maximum temperature rise is 60°C, and the temperature difference control range is ± 1.5°C.

2.2. Fuel Characteristic Analysis and Calculation. The high-efficiency fuel oil submersible hot water machine uses 0# diesel as fuel. According to the percentage of each component of 0# diesel, the theoretical air volume V^0 consumed when 1 kg of 0# diesel is completely burned under standard conditions can be calculated. And the volume of produced CO_2, SO_2, N_2, H_2O, and triatomic gas RO_2 and the volume of flue gas V_y are shown in Table 1 [9].

2.3. Enthalpy of Fuel Flue Gas. When 0# diesel and air are sent to the water heater for combustion, the heat carried is composed of two parts: one is the enthalpy brought by 0# diesel and air and the other is the chemical heat of 0# diesel itself. Therefore, it is necessary to calculate the enthalpy of fuel gas and the enthalpy of air [10].

The enthalpy value of 0# diesel flue gas is calculated based on 1 kg of 0# diesel, and it is calculated from 0°C. When the temperature is t°C, the enthalpy value I_y^0 of the theoretical flue gas volume is shown as follows:

$$I_y^0 = \left(V_{RO_2} C_{RO_2} + V_{N_2} C_{N_2} + V_{H_2O} C_{H_2O} \right) t, \qquad (1)$$

where V_{RO_2} is the theoretical triatomic gas RO_2 volume, m³/kg; C_{RO_2} is the average volume heat capacity of theoretical triatomic gas RO_2 at constant pressure, kJ/m³·k; V_{N_2} is the theoretical N_2 volume, m³/kg; C_{N_2} is the theoretical N_2 average volume heat capacity at constant pressure, kJ/m³·k; V_{H_2O} is the theoretical water vapor H_2O volume, m³/kg; C_{H_2O} is the average volume heat capacity of theoretical water vapor H_2O at constant pressure, kJ/m³·k; and t is the flue gas temperature, °C.

It can be seen from the above calculation that the theoretical SO_2 volume ratio is very small, so $C_{RO_2} = C_{CO_2}$ can be

used in the calculation. The enthalpy value of the theoretical air volume I_y^0 is shown as follows:

$$I_k^0 = V^0 C_k t_k, \qquad (2)$$

where V^0 is the theoretical air volume of the hot water machine, m³/kg; C_k is the average volume heat capacity of air at constant pressure, kJ/m³·k; and t_k is the air temperature, °C.

The flue gas enthalpy value I_y is shown as follows:

$$I_y = I_y^0 + (\alpha - 1) I_k^0, \qquad (3)$$

where I_y^0 is the enthalpy value of the theoretical flue gas volume of the hot water machine, kJ/m³; α is excess air coefficient; and I_k^0 is the enthalpy of theoretical air volume, kJ/m³.

The specific heat of each temperature of air and flue gas is shown in Table 2. The excess air coefficient is 1.1, and the calculation results of equations (1) and (2) are substituted into equation (3) to obtain the flue gas enthalpy as shown in Table 3.

3. Analysis of the Heat Balance of the Oil-Fired Submersible Hot Water Machine System

In order to ensure that the heat enters the hot water machine, the effective utilization of the hot water machine and the heat loss of the hot water machine reach a certain balance, so the heat balance calculation of the hot water machine system is required. After completing the heat balance calculation, the thermal efficiency of the hot water machine system and the consumption of the hot water machine per hour should be obtained initially, so that the subsequent structural design of the fuel-based submersible hot water machine can be carried out. The heat balance calculation of the oil-fired submersible hot water machine is based on the operation of the hot water machine system under stable thermal conditions. In the standard state, the calculation is based on the complete combustion of 1 kg of 0# diesel.

3.1. The Input Heat of the Fuel Submersible Hot Water Machine. Since 0# diesel fuel produces very little ash and can be ignored, so $Q_6 = 0$. At the same time, when 0# diesel is atomized and then burned, incomplete solid combustion will not occur, so $Q_4 = 0$. Therefore, the heat balance equation can be written as follows:

$$Q_r = Q_1 + Q_2 + Q_3 + Q_5, \qquad (4)$$

where Q_r is 1 kg of 0# diesel fuel sent to the heat of the submersible hot water machine system, $Q_r = 42900$ kJ/kg; Q_1 is the efficient use of heat in the hot water machine system, kJ/kg; Q_2 is the heat loss during exhaust of the hot water machine, kJ/kg; Q_3 is the heat lost when the oil mist of the hot water machine is incompletely burned, kJ/kg; and Q_5 is the heat transferred from the hot water machine system to the surrounding environment, kJ/kg.

Table 1: Summary table of smoke composition.

Data name	Code name	Unit	Value
Theoretical air volume	V^0	m^3/kg	11.153276
Theoretical flue gas	V_y	m^3/kg	12.086479
Theoretical CO_2 volume	V_{CO_2}	m^3/kg	1.596363
Theoretical SO_2 volume	V_{SO_2}	m^3/kg	0.001750
Theoretical N_2 volume	V_{N_2}	m^3/kg	8.811408
Theoretical triatomic gas RO_2 volume	V_{RO_2}	m^3/kg	1.598113
Theoretical water vapor H_2O volume	V_{H_2O}	m^3/kg	1.676958
Theoretical CO_2 volume ratio	r_{CO_2}	%	13.21
Theoretical SO_2 volume ratio	r_{SO_2}	%	0.01
Theoretical N_2 volume ratio	r_{N_2}	%	72.90
Theoretical RO_2 volume ratio	r_{RO_2}	%	13.22
Theoretical water vapor H_2O volume ratio	r_{H_2O}	%	13.87

Table 2: Specific heat table of air flue gas.

Temperature (°C)	Specific heat of combustion products of various gases (Kcal/m³·°C) Natural gas, coke oven gas, mixed gas, liquid fuel bituminous coal, and anthracite	Specific heat of air (Kcal/m³·°C)
0–200	0.33	0.31
200–400	0.34	0.31
400–700	0.35	0.32
700–1000	0.36	0.33
1000–1200	0.37	0.34
1200–1500	0.38	0.35
1500–1800	0.39	0.35
1800–2000	0.40	0.36

Table 3: Flue gas enthalpy temperature table.

Temperature (°C)	Theoretical smoke enthalpy I_y (kJ/m³)	Air enthalpy I_k (kJ/m³)	Flame tube outlet $\alpha'' = 1.1\ I_y$ (kJ/m³)	Smoke pipe outlet $\alpha_{py} = 1.1\ I_y$ (kJ/m³)
15	250	222	272	272
50	833	738	907	907
100	1666	1477	1814	1814
120	2007	1776	2185	2185
200	3372	2971	3669	3669
300	5123	4491	5572	5572
400	6923	6043	7527	7527
450	7847	6836	8531	8531
500	8771	7630	9534	9534
600	10667	9254	11592	11592
700	12612	10911	13703	13703
800	14599	12593	15858	15858
850	15609	13448	16954	16954
900	16619	14302	18050	18050
1000	18673	16031	20277	20277
1100	20760	17788	22539	22539
1200	22872	19556	24828	24828
1300	25012	21350	27147	27147
1400	27167	23156	29483	29483
1500	29344	24971	31841	31841
1600	31539	26800	34219	34219
1700	33753	28634	36617	36617
1750	34864	29552	37819	37819
1800	35974	30470	39021	39021
1900	38206	32331	41440	41440
2000	40451	34181	43869	43869

If the heat balance equation of the oil-fired submersible hot water machine is expressed by the percentage of each heat in the total heat input of the system, it can be written as shown in the following equation:

$$q_1 + q_2 + q_3 + q_5 = 100\%, \tag{5}$$

where q_i is the percentage of each heat to the total heat input to the system, $q_i = Q_i/Q_r \times 100\%$, %; q_1 is the heat utilization rate that the hot water machine effectively utilizes, %; q_2 is the exhaust smoke loss rate generated when the hot water machine exhausts the smoke, %; q_3 is the loss rate of incomplete combustion of the hot water machine oil mist, %; and q_5 is the heat loss rate of the hot water machine, %.

3.2. Exhaust Heat Loss.

Exhaust heat loss is the most important heat loss in the entire oil-fired submersible hot water machine system. Among them, the temperature and volume of the exhaust are important factors that affect the heat loss of the exhaust. For a certain quality of fuel, the value of the excess air coefficient determines the amount of smoke emitted, and the combustion state directly affects the size of the excess air coefficient.

The exhaust heat loss q_2 can be expressed by the difference between the enthalpy of the flue gas discharged from the hot water machine system and the enthalpy of the cold air, which can be written as follows:

$$q_2 = \frac{\left(I_{py} - \alpha_{py} I_{lk}^0\right)\left(100 - q_4\right)}{Q_r} \times 100\%, \tag{6}$$

where I_{py} is the enthalpy of the flue gas discharged after the combustion of 1 kg of 0# diesel under the excess air coefficient of the flue gas and the flue gas temperature, kJ/m^3; α_{py} is excess air coefficient of exhaust flue gas; and I_{lk}^0 is, at the temperature of the air entering the hot water machine, the enthalpy of the theoretical air required when 1 kg of 0# diesel is burned, kJ/m^3.

According to the research [11], the exhaust gas temperature is 200°C, and the temperature of the cold air sent to the hot water machine is 20°C, taking the excess air coefficient $\alpha_{py} = 1.1$ and substituting the value calculated according to Table 3 into equation (6). It can be obtained that the heat loss of exhaust gas of the oil-fired submersible water heater is $q_2 = 7.10\%$.

3.3. Incomplete Combustion of Oil Mist Heat Loss.

The heat loss of incomplete combustion of oil mist refers to the incomplete combustion of the 0# diesel after atomization. This part of the incompletely burned oil mist will directly reduce the total heat input to the oil-fired submersible hot water machine system. However, according to the actual situation, under the current technical control, as long as the combustion is good, the heat loss of this part can be controlled within a small range. In the design calculation, $q_3 = 1.25\%$.

3.4. The Effective Use of Heat of the Oil-Fired Submersible Hot Water Machine.

The effective heat utilization of the oil-fired submersible hot water machine refers to the difference between the total enthalpy of the flue gas produced by the combustion of 0# diesel and the enthalpy of the medium water input to the hot water machine. For the fuel submersible hot water machine, its effective use of heat Q_1 is shown as follows:

$$Q_1 = Gc_s\left(t_{rs} - t_{hs}\right), \tag{7}$$

where G is the flow rate of circulating water, kg/s; t_{rs} is the temperature of the hot water, °C; t_{hs} is backwater temperature, °C; and c_s is the specific heat of water, MJ/(kg·°C), generally taken $c_s = 0.0041868$MJ/(kg·°C).

According to the original design data of the fuel-burning submersible hot water machine in Section 2.1, substituting equation (7), the effective heat Q_1 of the fuel-burning submersible hot water machine can be calculated as 0.23 MW.

3.5. The Heat Loss of Fuel Oil Submersible Hot Water Machine.

The heat dissipation loss of the oil-fired submersible hot water machine refers to the heat that the hot water machine system loses to the outside of the environment under the action of the surrounding environment. The heat loss of the oil-fired submersible hot water machine is designed and calculated according to the relevant standards provided in TSG G0003-2010 "Industrial Boiler Energy Efficiency Testing and Evaluation Rules" [12], as shown in Table 4.

According to the calculation result of equation (7) and the data in Table 4, it can be seen that $q_5 = 2.1\%$.

3.6. Thermal Efficiency and Fuel Consumption of the Oil-Fired Submersible Hot Water Machine.

The thermal efficiency of the oil-fired submersible hot water machine is shown as follows:

$$\eta = 100 - (q_2 + q_3 + q_5), \tag{8}$$

where q_2 is the smoke loss rate during smoke exhaust, %; q_3 is the loss rate when incomplete combustion of oil mist occurs, %; and q_5 is the heat loss rate of hot water machine, %.

Substituting the q_2, q_3, and q_5 obtained above into equation (8), $\eta = 89.55\%$ is obtained. The fuel consumption of the oil-fired submersible hot water machine is shown as follows:

$$B = \frac{Q_1}{\eta Q_r} \times 100, \tag{9}$$

where Q_1 is the effective use of heat by hot water machine, MW; η is the thermal efficiency of the hot water machine, %; and Q_r is the heat sent to the submersible hot water machine system, kJ/kg.

Substituting the calculated values into equation (9), $B = 21.55$ kg/hcan be obtained.

When calculating the heat of oil-fired boilers, the volume of flue gas is used to calculate the temperature enthalpy table, so the heat calculation should be calculated by calculating the fuel consumption. The fuel consumption is calculated as shown in the following equation:

$$B_j = B\frac{100 - q_4}{100}, \qquad (10)$$

where B is the fuel consumption of the hot water machine, kg/h, and q_4 is the heat loss rate when solid fuel is incompletely burned, %.

Substituting $q_4 = 0$ and the value of equation (9) $B = 21.55$ kg/h into equation (10), $B_j = 21.55$ kg/h is obtained.

4. The Overall Structure Design of the Fuel-Type Submersible Hot Water Machine

The overall structure of the oil-fired submersible hot water machine includes the boiler tube, flame tube, smoke chamber, fire tube, bracket, flange, and flange cover, etc. The connecting parts of each part are selected by general standard parts to meet the interchangeability during maintenance reduces the maintenance cost of the hot water machine. For some nonuniversal standard parts, they are required to be designed.

The oil-fired submersible hot water machine adopts the central flame-return structure in the horizontal structure. After the flame is sprayed from the burner, the special structure of the flame tube will form an entrainment phenomenon, and the high-temperature smoke in the tube will continuous movement to the wall of the flame tube can form a very uniform temperature field, which is beneficial to heating the working fluid [13–15] as shown in Figure 1.

The burner of the oil-fired submersible water heater is the heating device of the hot water machine. As the core component of the hot water machine heating [16], when the burner is selected, there must be a corresponding value when meeting the basic power consumption [17]. According to the working characteristic curve of the burner, the working point of the burner must be in its corresponding full-load area, and the closer the working point is to the right side of the working curve, the better. The burner work curve is shown in Figure 2, and the final selected burner model is the UNIGAS LO280 AB burner.

The flame tube is designed according to the parameters of the selected burner. The flame tube consists of three parts, namely, the flange, the cylinder, and the head, which are connected by welding. The head adopts a standard elliptical head, and the flanging is to ensure the stability when connecting with the front smoke chamber, and the flame tube structure is shown in Figure 3.

The smoke chamber is a structure for storing high-temperature flue gas. The structure used in this article is the central flame-back type. The smoke chamber of the central flame-back hot water machine is arranged inside the drum. This structure can effectively reduce the heat loss. The smoke chamber has two parts, namely, the front smoke chamber and the rear smoke chamber. The front smoke chamber is connected with the flame tube, the threaded tube, and the inlet of the burner, and the rear smoke chamber is connected with the threaded tube and the chimney. The structures of the front smoke chamber and the rear smoke chamber are shown in Figures 4 and 5.

TABLE 4: Boiler heat loss table.

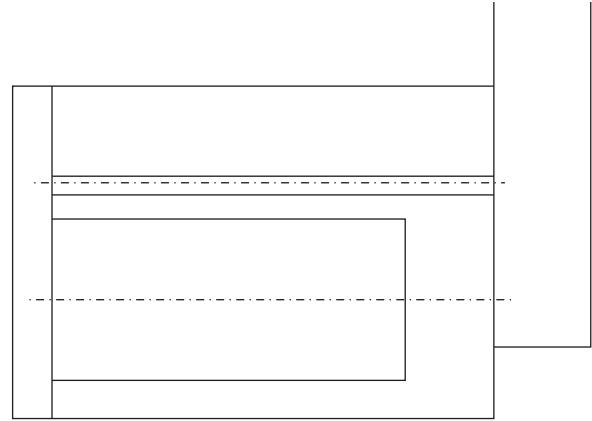| Boiler rated output		≤4	6	10	15	20	35	≥65
	t (h)	≤4	6	10	15	20	35	≥65
	MW	≤2.8	4.2	7.0	10.5	14	29	≥46
Heat loss	%	2.1	2.4	1.7	1.5	1.3	1.1	0.8

FIGURE 1: Schematic diagram of the central flame-return structure of a horizontal hot water machine.
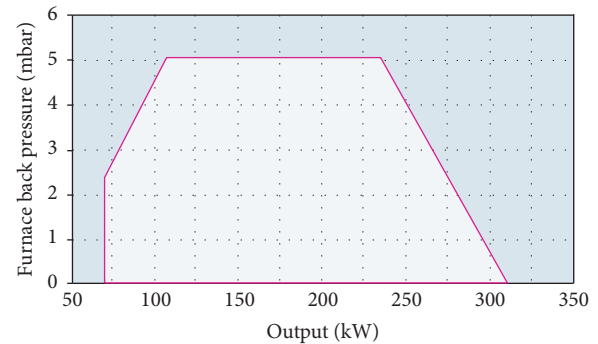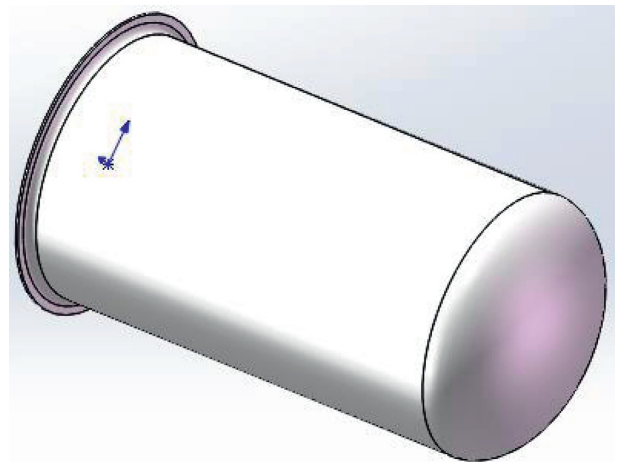

FIGURE 2: Burner working curve.

FIGURE 3: Structure diagram of the flame tube.

The central flame-back water heater is equipped with threaded pipes, and the number of threaded pipes and the pipe distance have strict requirements. The threaded tube is
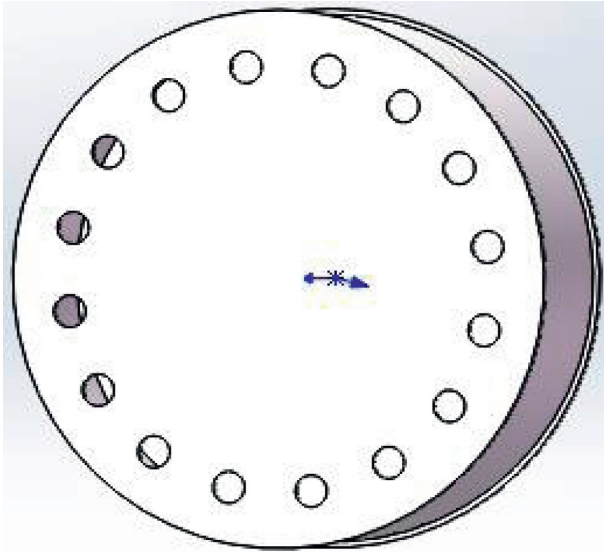
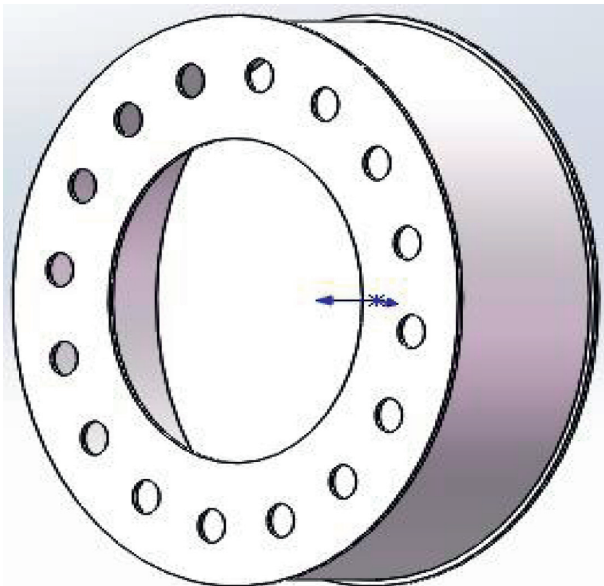Figure 4: Structure of the front smoke chamber.

Figure 5: Structure diagram of the rear smoke chamber.

formed by rolling and forming an ordinary smooth tube. The purpose of increasing the thread is to enhance the intensity of turbulence in the tube and enhance the convective heat transfer capacity of flue gas. The size of the threaded pipe is ф 32 × 710, and the size of the flange is designed according to the outer diameter of the drum.

The drum is designed according to the volume of the water heater. The design capacity of the drum in this article is 250 L. When designing the drum, a partition was added to the back half of the drum. The purpose of adding the partition was two: one is to provide support for the rear smoke chamber, and the other is to separate the hot and cold water. The drum structure is shown in Figure 6.
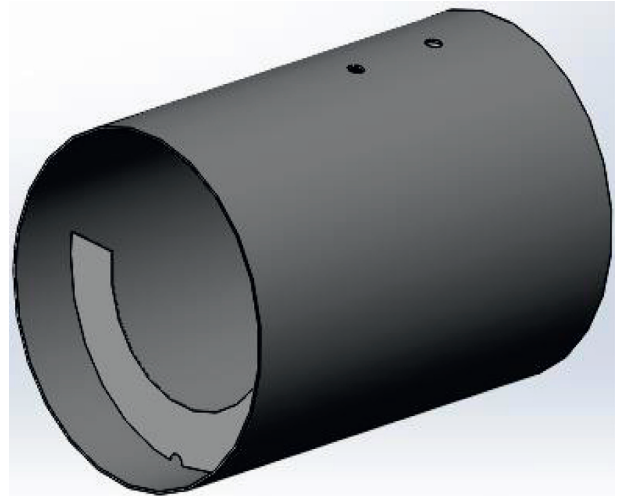

Figure 6: Drum structure diagram.

5. Heat Transfer Calculation of Flame Tube of the Oil-Fired Submersible Hot Water Machine

5.1. Basic Data Calculation of the Hot Water Machine. The total area of the furnace wall on each side of the flame tube $F_b = \pi \times (0.394)^2 + \pi \times 0.788 \times 1.2 = 3.946 \, \text{m}^2$.

Since the flame tube is composed of a head and a cylinder, the covering area is not a conventional surface. Since the three-dimensional structure model of the flame tube has been established, the covering area $F_l = 0.595 \, \text{m}^2$ of the flame tube can be obtained through software calculation.

Similarly, the volume of the flame tube is not a conventional volume. Using software calculations, the volume of the flame tube $V_l = 0.041 \, \text{m}^3$ can be obtained.

5.2. The Effective Radiation Heating Area in the Boiler of the Oil-Fired Submersible Hot Water Machine. The effective radiation heating area in the boiler of the oil-fired submersible hot water machine can be obtained by the following equation:

$$H_f = xF_b, \tag{11}$$

where x is the effective angle factor and F_b is the area of the boiler wall where the water wall is arranged, m^2.

Because the flame sprayed by the burner radiates all the heat to the wall of the flame tube, the effective angle factor is 1. Therefore, substituting the values of F_b and x into equation (11), it can be known that the effective radiation heating area in the boiler of the hot water machine is $H_f = 3.946 \, \text{m}^2$.

5.3. The Effective Radiation Heating Area in the Boiler of the Oil-Fired Submersible Hot Water Machine. The effective heat release of the fuel-type submersible hot water machine can be obtained by the following equation:

$$Q_l = Q_r \times \frac{100 - q_3 - q_4 - q_6}{100 - q_4} + Q_k, \tag{12}$$

where Q_r is the heat sent to the hot water machine, kJ/kg; q_3 is loss rate when incomplete combustion of oil mist occurs, %; q_4 is the heat loss rate of incomplete combustion of solid fuel, %; q_6 is the heat loss rate taken away by the ash in the fuel, %; and Q_k is the amount of heat in the air required for combustion, kJ/kg.

When the fuel is burned, the heat required to send the air into the hot water machine is as shown in the following equation:

$$Q_k = a_l'' I_{rk}^0, \qquad (13)$$

where a_l'' is excess air coefficient at the outlet of the flame tube of the hot water machine and I_{rk}^0 is the enthalpy of the air entering the flame tube of the hot water machine, kJ/kg.

According to the research, take $a_l'' = 1.1$, and select the enthalpy value of the outlet air $I_{rk}^0 = 295$ kJ/kg. Substituting the selected value into equation (13), we can obtain $Q_k = 324.5$ kJ/kg, and substituting the obtained Q_k and the previously calculated values into equation (12), the effective heat output of the water heater can be obtained as $Q_l = 42688$ kJ/kg.

Querying the smoke enthalpy table shows that the absolute combustion temperature corresponding to the effective heat release Q_l is $\theta_u = 1953°C$, so the absolute combustion temperature $T_u = \theta_u + 273 = 2226$ K.

5.4. Calculation of the Flame Blackness of the Oil-Fired Submersible Hot Water Machine and the Flame Blackness of the Flame Tube.
When the fuel is liquid, the flame blackness is formed by the superposition of the blackness of the luminous part of the flame and the blackness of the nonluminous part. The blackness of the luminous part of the flame and the blackness of the nonluminous part of the flame are, respectively, represented by the following equations:

$$a_{fg} = 1 - e^{-\left(k_q r_q + k_{th}\right)PS}, \qquad (14)$$

$$a_{bfg} = 1 - e^{-k_q r_q PS}, \qquad (15)$$

where k_q is the triatomic gas radiation attenuation coefficient, $1/(m \cdot MPa)$; r_q is the volume share of flame triatomic gas, %; k_{th} is the flame carbon black particle radiation attenuation coefficient, $1/(m \cdot MPa)$; P is flame tube pressure, MPa; and S is the effective radiation layer thickness, m.

The effective radiation thickness is shown as follows:

$$S = 3.6 \frac{V_l}{F_l}, \qquad (16)$$

where V_l is the effective volume of hot water machine flame tube, m^3, and F_l is the covering area of the flame tube of the hot water machine, m^2.

Substituting the values of the effective volume V_l of the flame tube and the coating area F_l of the flame tube into formula (16), the value of the effective radiation thickness can be obtained as $S = 0.248$ m.

The radiation attenuation coefficient of triatomic gas is shown as follows:

$$k_q = 10 \left(\frac{0.78 + 1.6 r_{H_2O}}{\sqrt{10 P_q S}} - 0.1 \right) \left(1 - 0.37 \frac{T_l''}{1000} \right), \qquad (17)$$

where r_{H_2O} is the volume ratio of water vapor to flue gas, %; P_q is the total partial pressure of the triatomic gas in the flame, MPa; S is the effective radiation thickness, m; and T_l'' is the smoke temperature at the exit of the flame tube, °C.

Since the high-efficiency fuel oil submersible hot water machine works in a normal pressure environment, $P_q = 0.1$ MPa is taken. When the water heater is designed, the flue gas temperature at the outlet of the flame tube is set to 980°C, that is, $T_l'' = 980°C$. Substituting the corresponding values into equation (17), we can get $k_q = 12.11$.

Substituting the corresponding values, the blackness of the luminous part of the flame $a_{fg} = 0.019$ and the blackness of the nonluminous part of the flame $a_{bfg} = 0.412$.

5.5. Calculation of Heat Release and Heat Transfer of Flame Tube Flue Gas of the Oil-Fired Submersible Hot Water Machine.
The heat release of the flue gas from the flame tube is shown as follows:

$$Q_{rp} = \varphi \left(Q_l - I_l'' \right), \qquad (18)$$

where ϕ is the heat preservation coefficient, %; Q_l is the heat of the flame tube, kJ/kg; and I_l'' is the enthalpy value corresponding to the flue gas temperature at the outlet of the flame tube, kJ/kg.

According to this research, setting the outlet temperature of the flame tube $k_l'' = 477°C$, the corresponding smoke enthalpy $I_l'' = 8346$ kJ/kg. Substituting the corresponding values into equation (18), the heat release of the flame tube flue gas is $Q_{rp} = 33552.1$ kJ/kg.

The heat transfer of the flue gas in the flame tube is shown as follows:

$$Q_{cr} = C \frac{H_f}{B_j} \left[\left(\frac{T_{hy}}{100} \right)^4 - \left(\frac{T_b}{100} \right)^4 \right], \qquad (19)$$

where C is the radiation and convection heat transfer coefficient, take $C = 11.72$ kW/(m²·K); B_j is the fuel consumption of the hot water machine, kg/h; T_{hy} is the average flame temperature, K; and T_b is the surface temperature of the water wall, K.

Substituting the corresponding values into equation (19), the heat transfer amount of the flame tube flue gas can be obtained as $Q_{cr} = 33573.7$ kJ/kg.

The calculation error of the flame tube of the hot water machine is shown as follows:

$$\Delta = \left| \frac{Q_{rp} - Q_{cr}}{Q_{rp}} \right| \times 100 = \left| \frac{33552.1 - 33573.7}{33552.1} \right| \times 100 = 0.064\%. \qquad (20)$$

6. Calculation of Convective Heat Transfer in Hot Water Machine

Convection heat transfer is one of the important heat transfer methods of high-efficiency fuel-type submersible hot water machines. For high-efficiency fuel-type submersible hot water machines, the convective heating surface refers to the heating surface of the fire tube and smoke chamber of the hot water machine. In the heating surface of these hot water machine systems, heat is transferred to the medium water in a convective manner, and the calculation of convective heat transfer is also based on the heat released by the combustion of 1 kg of 0# diesel.

6.1. Basic Data Calculation of Convective Heat Transfer Surface.
The fire tube takes the form of a threaded tube, which can improve the heat exchange efficiency to a certain extent, so that the medium absorbs more heat. The steel pipe is a standard steel pipe with a diameter of 32 mm and a thickness of 2.5 mm. The threaded pipe is pressed by a special threaded pipe with a guide rail bracket. The front and rear smoke chambers have smooth walls and cylindrical structures. The specific parameters are shown in Table 5.

According to the data in Table 5, the flue gas flow area Fr of the threaded tube, the heat transfer area Hr of the threaded tube, the heat transfer area Hs of the fume chamber, and the total flue gas flow area Fd can be further obtained. The total heat transfer area Hd is shown in Table 6.

6.2. Calculation of Heat Release of Flue Gas.
The amount of heat emitted by the flue gas is shown as follows:

$$Q_{rp} = \varphi((I' - I''), \tag{21}$$

where φ is the heat preservation coefficient; I' is the enthalpy of inlet flue gas, kJ/kg; and I'' is the enthalpy of outlet flue gas, kJ/kg.

Now set the inlet flue gas temperature Θ' to 477°C, check the flue gas enthalpy table, its corresponding enthalpy value $I' = 8328$ kJ/kg, the flue gas outlet temperature $\Theta'' = 200°C$, and its corresponding enthalpy value $I'' = 3372$ kJ/kg. The previously calculated heat preservation coefficient $\varphi = 0.977$. Therefore, the calorific value of the flue gas is $Q_{rp1} = 4842$kJ/kg.

6.3. Average Flue Gas Temperature, Flow Velocity, and Temperature and Pressure Calculation.
The average flue gas temperature is shown as follows:

$$\theta_p = \frac{\theta' + \theta''}{2}, \tag{22}$$

where Θ' is the inlet flue gas temperature, °C, and Θ'' is the outlet flue gas temperature, °C.

Substituting the corresponding values into equation (22), we can get $\theta_p = 338.5°C$.

The average flue gas flow rate is shown as follows:

Table 5: Convection surface structure parameter table.

Project name	Code name	Unit	Value
Threaded pipe pitch	t	mm	45
Threaded pipe groove depth	ε	mm	2
Threaded pipe inner diameter	dr	mm	29.5
Number of threaded pipes	Nr	—	16
Longitudinal scour length of threaded pipe	L	M	0.7
Front and rear smoke chamber diameter	ds	mm	520
Longitudinal scour length of smoke chamber	L'	M	0.4

Table 6: Convection surface structure parameter table.

Project name	Code name	Unit	Value
Threaded pipe flue gas flow area	Fr	m^2	0.011
Heat transfer area of threaded tube	Hr	m^2	1.038
Heat transfer area of smoke chamber	Hs	m^2	0.372
Total flue gas circulation area	Fd	m^2	0.011
Total heat transfer area	Hd	m^2	1.410

$$\omega = \frac{B_j V_y}{3600 Fd} \cdot \frac{\theta_p + 273}{273}, \tag{23}$$

where B_j is the fuel consumption of the hot water machine, kg/h; V_y is the theoretical flue gas, m^3/kg; Fd is the total flue gas circulation area, m^2; and Θ_p is the average flue gas temperature, °C.

Substituting the corresponding values obtained above into equation (23), the average flue gas flow velocity can be obtained as $\omega = 14.7$m/s.

The logarithmic temperature and pressure are shown as follows:

$$\Delta t = \frac{\Delta t_d - \Delta t_x}{\ln \Delta t_d / \Delta t_x}, \tag{24}$$

where Δt_d is the large end temperature, °C, and Δt_x is the small end temperature, °C.

Among them, the large end temperature and pressure value is the difference between the inlet flue gas temperature and the working fluid outlet temperature, that is, $\Delta t_d = \theta' - t_2 = 477 - 60 = 417°C$, and the small end temperature and pressure value is the difference between the outlet flue gas temperature and the working fluid inlet, that is, $\Delta t_x = \theta'' - t_1 = 200 - 4 = 196°C$, and substituting the values obtained above into equation (24), the logarithmic temperature and pressure can be obtained as $\Delta t = 284.4$.

6.4. Calculation of Convective Heat Transfer Coefficient.
The convective heat transfer coefficient is used to express the heat transfer capacity between the medium water and the convection surface. For high-efficiency oil-fired submersible hot water machines, the convection heat transfer surface has a fire tube and a smoke chamber. Therefore, it is necessary to calculate the total convective heat transfer coefficient of the flue gas.

The Prandtl coefficient of the flue gas $Pr = 0.6211$, the kinematic viscosity coefficient of the flue gas $v = 0.00009 \, m^2/s$, the thermal conductivity of the flue gas $\lambda = 0.0783 \, kW/(m\cdot°C)$, and the average flue gas flow rate $\omega = 14.7 \, m/s$, and it can be calculated that the Rayleigh number of the threaded tube $Rer = \omega dr/v = 14.7 \times 0.0295/0.00009 = 4818$, and the Rayleigh number of the smoke chamber $Res = \omega ds/v = 14.7 \times 0.52/0.00009 = 84933$.

The convective heat transfer coefficient of the threaded tube is shown as follows:

$$a_r = 0.0144 \left(\frac{t}{dr}\right)^{-0.08} \cdot \left(\frac{\varepsilon}{dr}\right)^{0.112} Rer^{0.926}, \qquad (25)$$

where t is the pitch of the threaded pipe, mm; dr is the inner diameter of the threaded pipe, mm; ε is the groove depth of the threaded pipe, mm; and Rer is the Reynolds number of the threaded pipes.

Substituting the corresponding values into equation (23), the convective heat transfer coefficient of the threaded tube $a_r = 0.026 kW/(m\cdot°C)$ can be obtained.

The convective heat transfer coefficient of the smoke chamber is shown as follows:

$$a_s = 0.023 \frac{\lambda}{ds} Res^{0.8} Pr^{0.4}, \qquad (26)$$

where λ is the thermal conductivity of flue gas, $kW/(m\cdot°C)$; ds is the inner diameter of the smoke chamber, mm; Res is the Reynolds number of the smoke chamber; and Pr is the Prandtl coefficient of flue gas.

Substituting the corresponding values into equation (26), the convective heat transfer coefficient of the smoke chamber $a_s = 0.025 kW/(m\cdot°C)$ can be obtained.

From the convective heat transfer coefficient of the threaded tube and the smoke chamber, the total convective heat transfer coefficient of the flue gas $a_d = (a_s Hs + a_r Hr)/Hs + Hr = 0.025 \times 0.372 + 0.026 \times 1.038/0.372 + 1.038 = 0.072 kW/(m\cdot°C)$. can be further calculated.

6.5. Calculation of Radiation Heat Release Coefficient of Flue Gas.

The radiation attenuation coefficient of triatomic gas is shown as follows:

$$k_q = \left(1 - 0.37 \frac{\theta_p + 273}{1000}\right)\left(\frac{2.47 + 5.06 r_{H_2O}}{\sqrt{r_q PS}} - 1\right) r_q, \quad (27)$$

where Θ_p is the average flue gas temperature, °C; r_{H_2O} is the volume ratio of water vapor to flue gas, %; r_q is the volume share of flame triatomic gas, %; P is the flame tube pressure, MPa; and S is the effective radiation layer thickness, m.

Substituting the corresponding values into equation (27), the radiation attenuation coefficient of triatomic gas $k_q = 2.050 \, (MPa \cdot m)^{-1}$ can be obtained. From the radiation

attenuation coefficient of triatomic gas, the smoke blackness $a_y = 1 - e^{-k_q PS} = 1 - e^{-2.050 \times 1 \times 0.248} = 0.400$ can be further obtained.

The temperature ratio is shown as follows:

$$\tau = \frac{t_b + 273}{\theta_p + 273}, \qquad (28)$$

where t_b is the surface temperature of the water wall, °C, and θ_p is the average flue gas temperature, °C.

The surface temperature t_b of the water wall is taken as 283°C, that is, $t_b = 283°C$, and then the temperature ratio $\tau = 0.793$. According to the obtained temperature ratio, the radiation heat release coefficient of the flue gas $a_f = 0.026$ can be further obtained.

6.6. Calculation of Heat Transfer and Heat Transfer Error of the Main Heating Surface.

The total heat transfer coefficient is shown as follows:

$$K = \psi(a_d + a_f), \qquad (29)$$

where ψ is the thermal effective coefficient; a_d is the total convective heat transfer coefficient of flue gas; and a_f is the radiative heat release coefficient of flue gas.

Thermal effective coefficient $\psi = 0.73$; substituting the corresponding values into equation (29), the total heat transfer coefficient can be obtained as $K = 0.73 \times (0.072 + 0.026) = 0.072$.

The heat of the main heating surface is shown as follows:

$$Q_{cr} = \frac{KH d\Delta t}{B_j}, \qquad (30)$$

where K is the total heat transfer coefficient; Hd is the total heat transfer area, m^2; Δt is the logarithmic temperature, °C; and B_j is the fuel consumption of the hot water machine, kg/h.

Substituting the corresponding values into equation (30), the heat of the main heating surface can be obtained as $Q_{cr} = 4822 kJ/kg$ and the heat transfer error of the main heating surface as $\Delta = |Q_{rp1} - Q_{cr}/Q_{rp1}| \times 100 = |4842 - 4822/4842| \times 100 = 0.41\%$.

6.7. Total Heat Balance Check of the Hot Water Machine.

The overall calculation error of the water heater is shown as follows:

$$\Delta Q = \frac{Q_r \eta}{100 - q_4} - Q_{rp} - Q_{rp1}, \qquad (31)$$

where Q_r is the total heat sent to the hot water machine system, kJ/kg; η is the thermal efficiency of the hot water machine, %; q_4 is the heat loss rate of incomplete combustion of solid fuel, %; Q_{rp} is the heat release of flame tube smoke, kJ/kg; and Q_{rp1} is the exothermic amount of flue gas, kJ/kg.

Substituting the corresponding values into equation (31), we can get the overall calculation error of the water heater $\Delta Q = 22.95\,kJ/kg$ and the overall relative calculation error of the hot water machine $\Delta = \Delta Q/Q_r \times 100 = 22.95/42900 \times 100 = 0.053\%$.

7. CAE Analysis of High-Efficiency Fuel Submersible Hot Water Machine

With the rise of computer-aided engineering, analyzing engineering problems in reality has become simple and quick [18]. For high-efficiency fuel-type submersible water heaters, the CAE analysis that needs to be done is mainly structural analysis and thermal analysis. In terms of structural analysis, the workbench is used to simulate the force of each main structure, so as to better predict the quality problems of the water heater before the manufacturing is completed.

7.1. CAE Analysis of Drum. The drum is made of 316 L stainless steel with a thickness of 3.5 mm. There are three holes with a diameter of 40 mm on the surface of the drum. The through pieces are connected to these three holes by welding. The other ends of the three through pieces are connected to the overflow: flow valve, float, and plug match. A support plate is also welded inside the drum. On the one hand, the support plate is used to support the rear smoke chamber, and on the other hand, it is used to isolate cold and hot water, so that the temperature of the hot water output in the hot water machine is more stable. The structure is shown in Figure 6.

It can be seen from Figure 7 that the maximum deformation of the drum is 0.41344 mm and the minimum deformation is 0 mm. The area with the largest amount of deformation is mainly concentrated on the two sides of the line connecting the centers of the two openings. The deformation area around the opening is more evenly distributed. The deformation around the overflow valve hole is 0.091875 mm, and the half side around the float joint hole is even deformed. The amount is 0 mm. After the penetration piece is welded to the hole, such a small amount of deformation ensures the stability of the drum. The recession in the opening area is because the strength of the barrel wall is reduced after the opening of the hole, and the inside of the barrel is subjected to pressure, which ultimately leads to the deformation of the barrel. It can be seen from Figure 8 that the stress distribution of the drum is relatively uniform, and there is stress concentration around the opening of the drum, which is a normal phenomenon. It can be seen from Figure 9 that the strain near the opening of the drum shows a symmetrical state. Since the deformation near the opening is larger than that of other regions, the strain in this part of the region is also larger than that in other regions. Since the maximum stress of the drum is far less than the allowable stress, the strength and rigidity of the drum fully meet the working requirements, and there is no need to optimize the structure of the drum.
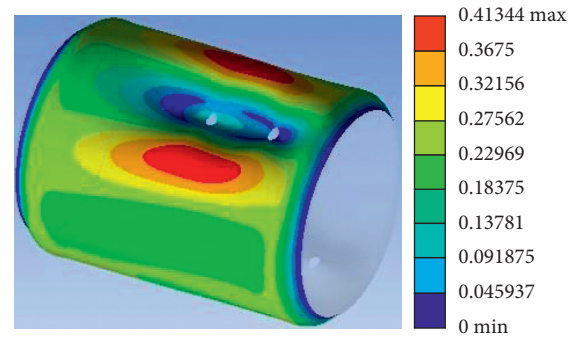

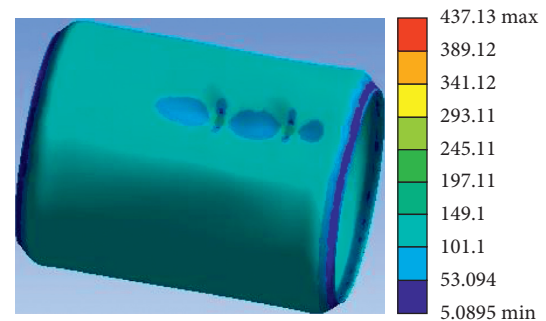FIGURE 7: Cloud diagram of total deformation of the drum.
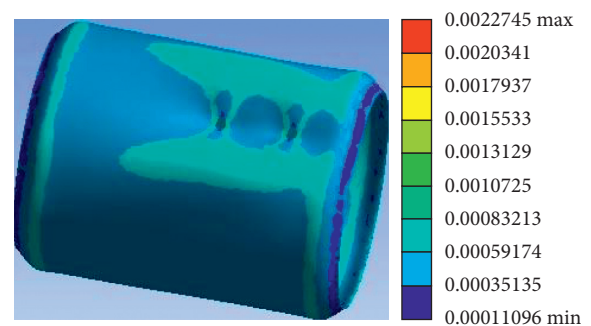

FIGURE 8: Equivalent stress cloud diagram of the drum.

FIGURE 9: Equivalent strain cloud diagram of the drum.

7.2. Flange CAE Analysis. The flange is an important part to connect the drum and the end cover, and the flange and the drum are connected by welding. The material of the flange is 316 L stainless steel. The three-dimensional view of the flange is shown in Figure 10.

The flange is meshed, and the mesh size is selected as 10 mm, and then the simulation is performed.

The flange inner ring and the drum are connected by welding, and the flange and the end cover are connected by bolts. The main bearing surface of the flange is the boss surface at the front end of the flange. This part of the area is in full contact with the gasket, and the force received comes from the internal pressure of the drum. The round hole on the flange end face matches the bolt, so the inner face of the round hole is subjected to shearing force. The total deformation cloud diagram of the flange is shown in Figure 11. The deformation area of the flange is mainly concentrated on
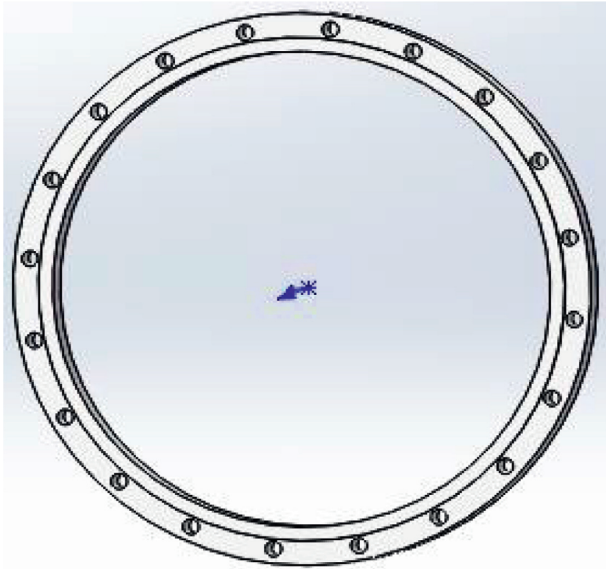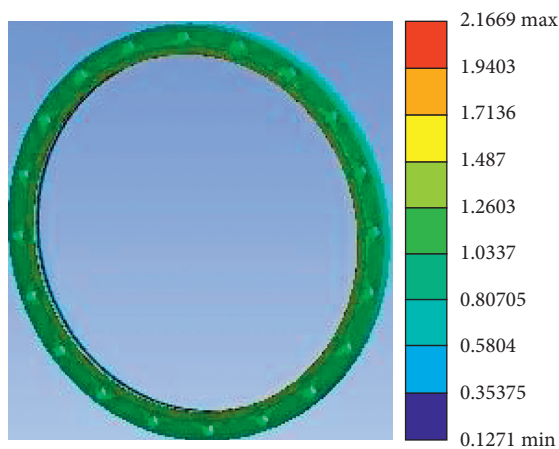
FIGURE 10: Three-dimensional view of the flange.

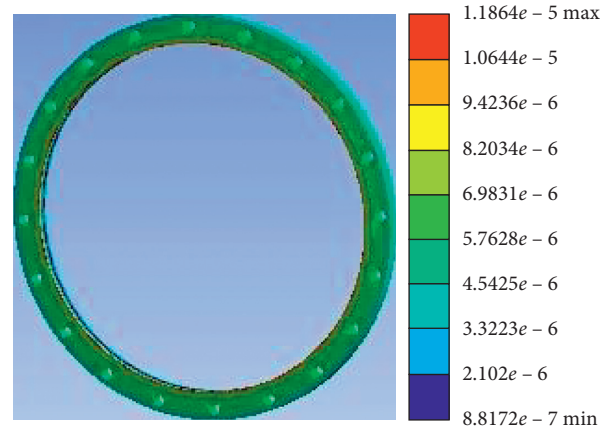FIGURE 11: Cloud diagram of total flange deformation.

FIGURE 12: Equivalent stress cloud diagram of the flange.

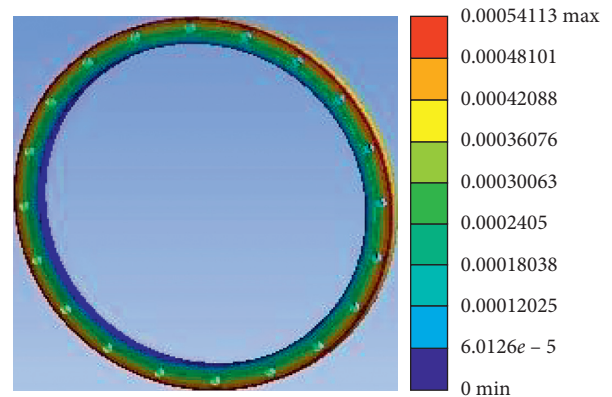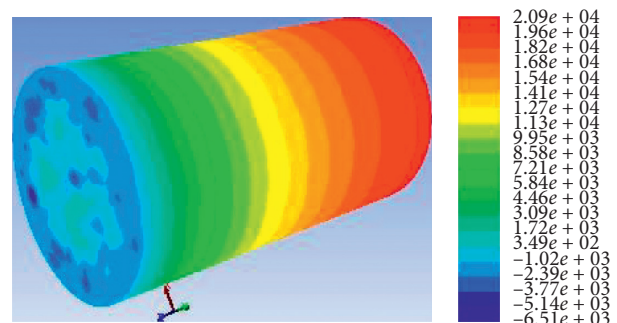FIGURE 13: Equivalent strain cloud diagram of the flange.

FIGURE 14: Pressure cloud diagram of the flame tube.

the edge of the flange, and the edge of the flange is relatively weak compared to other parts and is compressed by the bolt connection, so the deformation range of the region is larger than that of other regions. The stress and strain cloud diagrams of the flange are shown in Figures 12 and 13. From the cloud diagrams, the stress and strain distribution of the flange is very uniform and the values are very small. Therefore, the physical properties of the flange are very good.

7.3. Thermal Field Analysis of Flame Tube. The flame tube is the core thermal reaction element of the entire hot water machine. After the burner sprays the flame, the entire heating process of the hot water machine is carried out in the flame tube [19], so the thermal field of the flame tube is analyzed and studied. It is particularly important.

Using fluent software can simulate the state of the thermal field more accurately and quickly. It can be seen from Figure 14 that the pressure of the flame tube gradually increases along the tail of the flame tube until the pressure at

the head reaches the maximum. At the entrance of the flame tube, the center pressure of the flame tube is greater than the pressure around the flame tube, and the pressure around the flame tube is lower than the center pressure of the flame tube, forming an entrainment effect. It is precisely because of the entrainment effect that the heat of the flame tube is more uniform and the heat exchange efficiency is more efficient. It can be seen from Figure 15 that the temperature in the back half of the flame tube is in a stable state. Because the front wall of the flame tube has a shorter distance from the flame, the radiation intensity of the flame is also greater, so the temperature is higher. Figure 16 shows the change in the
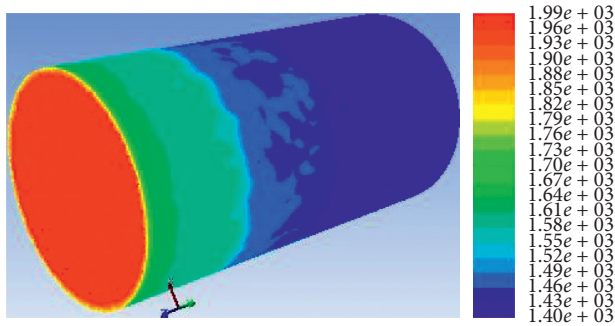
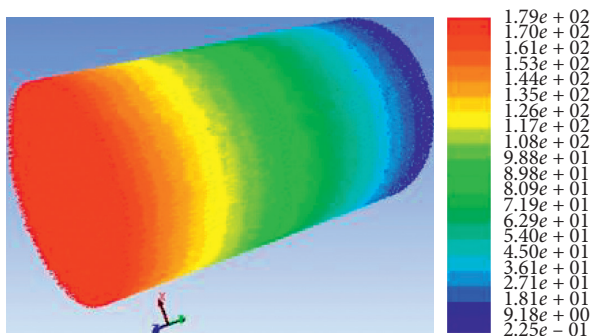FIGURE 15: Temperature cloud diagram of the flame tube.

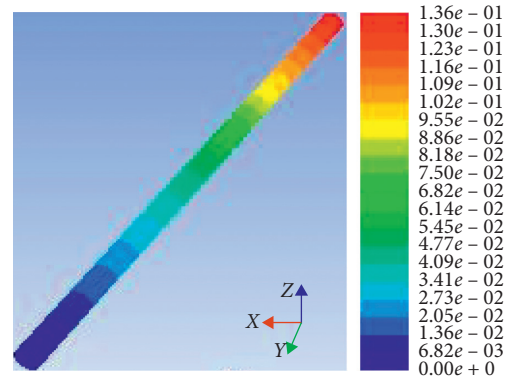FIGURE 16: Flame cylinder velocity vector cloud diagram.
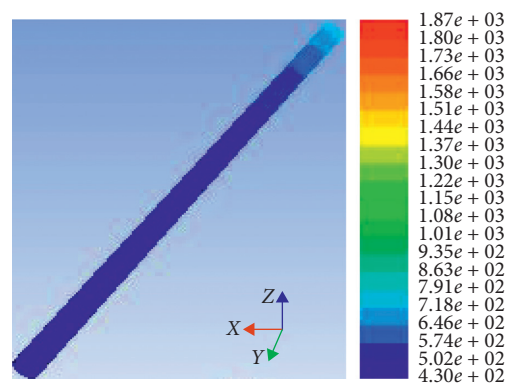

FIGURE 17: Pressure cloud diagram of the threaded pipe.

FIGURE 18: Temperature cloud diagram of the threaded pipe.

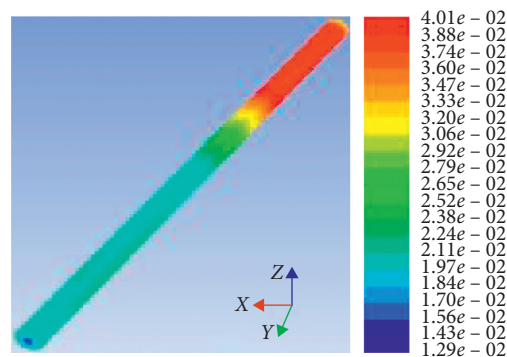FIGURE 19: Speed vector cloud diagram of the threaded pipe.

smoke velocity of the flame tube. The flame injected by the burner enters the flame tube from the entrance of the flame tube. The flue gas blocks the descending speed at the head of the flame tube and then turns back and enters from the inner cavity of the flame tube.

7.4. Thermal Field Analysis of Threaded Pipe. The threaded tube is one of the main components of the flue gas scouring. After the high-temperature flue gas is discharged from the flame tube, it enters the front smoke chamber, then enters the rear smoke chamber through the threaded tube, and is finally discharged into the atmosphere. As the main component of the flue gas scouring, the threaded tube is also very important to study its thermal field [20].

The fluent software is also used to simulate the thermal field. It can be seen from Figure 17 that the upper end of the threaded tube is the flue gas inlet, and the gas pressure gradually decreases from the inlet to the outlet. The inlet pressure is large and the outlet pressure is small, so that the flue gas can continuously flow from the inlet to the outlet. It can be seen from Figure 18 that the temperature distribution of the threaded pipe is relatively uniform, the temperature at the inlet end is higher, and the temperature at the outlet end decreases. The flue gas transfers heat to the threaded pipe wall in two forms of convection heat exchange and radiation heat exchange, and the threaded pipe wall transfers the heat to the working fluid water. It can be seen from Figure 19 that the threaded tube starts from the inlet, the first part of the flue gas velocity is relatively large, and as the length of the threaded tube increases, the resistance of the flue gas also increases, so the flue gas velocity decreases.

8. CAE Analysis of High-Efficiency Fuel Submersible Hot Water Machine

The flame tube is the component with the largest temperature difference of the oil-fired hot water machine. In the analysis, not only the influence of the static field on the flame tube must be considered, but also the change in the intensity of the flame tube under the thermal field coupling. It is very important to conduct multifield coupling analysis on the flame tube [21]. The thermal structure coupling analysis is completed in the workbench software. In the above, the thermal field of the flame tube flue gas was studied, and this section focuses on the thermal field of the flame tube body.

The temperature cloud diagram of the flame tube body is shown in Figure 20. From Figure 20, it can be concluded that the temperature distribution of the flame tube body is extremely uniform. There are two reasons for this phenomenon: one is the entrainment of the smoke in the flame tube. The high-temperature flue gas moves uniformly on the wall of the flame tube, so that the temperature difference in the entire heat exchange process is small, and the flame tube body uniformly absorbs heat; second, the material of the flame tube is 316 L stainless steel, and the heat transfer coefficient of 316 L stainless steel is $16.3 \, W/(m^2 \cdot K)$, the material itself has better heat transfer performance, so the temperature distribution of the flame tube is even.

After the temperature field analysis of the flame tube body, the flame tube is statically analyzed on the basis of the original temperature field. For 316 L stainless steel, on the basis of the temperature field, static analysis can describe the actual state of the flame tube more objectively. From the three aspects of total deformation, stress, and strain, the flame tube occurs due to the effect of the temperature field. The total deformation can intuitively reflect the appearance deformation of the flame tube due to external force. The stress objectively shows the internal reaction of the flame tube to the outside world after the external force is applied. The strain objectively shows the relative deformation of the internal structure of the flame tube.

Figures 21 and 22 are the total deformation cloud diagrams of the flame tube in the uncoupled and coupled conditions, respectively. By comparison, it can be seen that, in the case of multifield coupling, the temperature field has a certain influence on the flame tube. The main deformation changes are concentrated in the middle of the flame tube and the top of the head. Due to the coupling and superposition of the temperature field, the deformation of these parts has changed to different degrees. For the middle part of the flame tube, in the case of no coupling, there are two deformation areas in the middle part of the flame tube, and the middle part of the flame tube deforms unevenly. In the case of multifield coupling, the middle part of the flame tube has the same amount of deformation. For the top of the head, the change in total deformation is also more obvious. The effect of the temperature field increases the deformation of the head of the flame tube, and the edge transition of the deformation also tends to be gentle. But for the flame tube that is only subjected to the static force field, the difference in the amount of deformation is relatively obvious, and the transition of the deformation edge is not obvious. The reason for this phenomenon is that the temperature field affects the material properties of 316 L stainless steel. Under the action of the temperature field, the plasticity of the stainless steel material increases and the rigidity decreases. When subjected to the same static force field, it exhibits different properties.

Figures 23 and 24 are the equivalent stress cloud diagrams of the flame tube in the uncoupled and coupled conditions, respectively. From these two cloud diagrams, it can be clearly seen that the temperature field has a greater influence on the stress of the flame tube. In the case of no
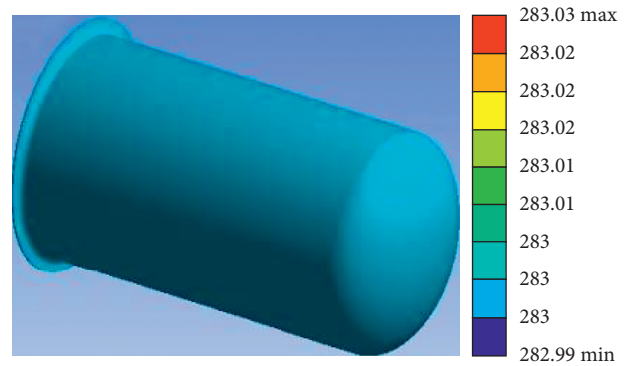

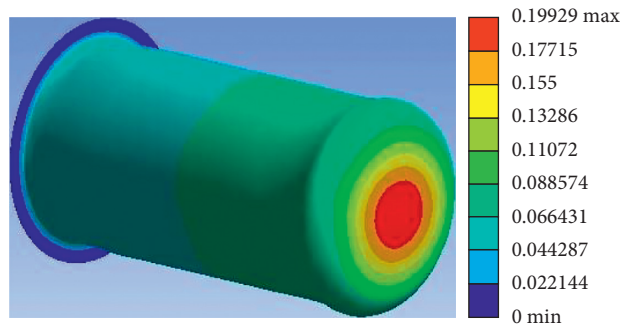FIGURE 20: Temperature cloud diagram of the flame tube body.

FIGURE 21: Total deformation cloud of the flame tube without coupling.
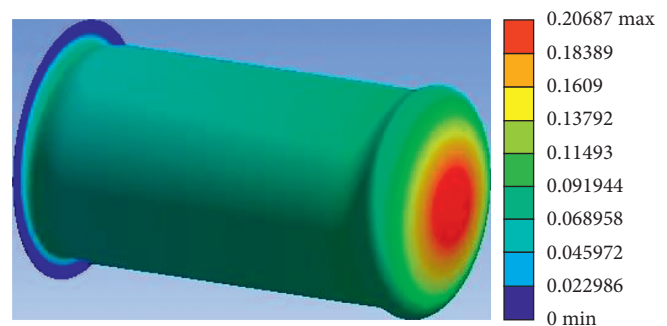

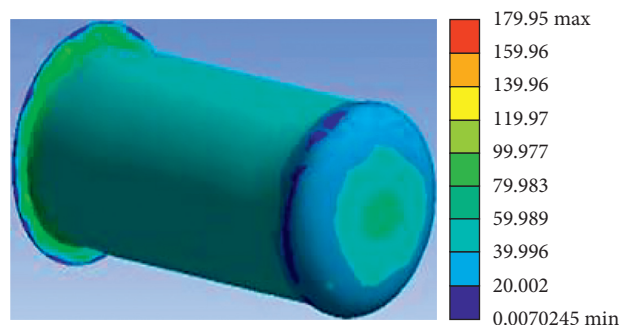FIGURE 22: The total deformation cloud diagram of the flame tube in the coupled case.

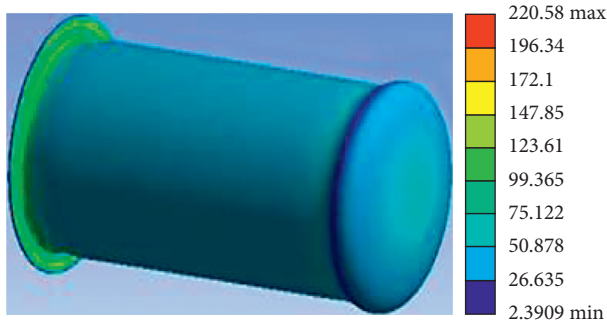FIGURE 23: Equivalent stress cloud diagram of the uncoupled flame tube.

FIGURE 24: Equivalent stress cloud diagram of the coupled flame tube.

FIGURE 25: Equivalent strain cloud diagram of the uncoupled flame tube.

coupling, the stress distribution in the head part of the flame tube is very uneven, and the stress in the top area of the head is relatively high, and the stress gradually decreases to the surroundings with the center of the head as the origin. In the case of multifield coupling, the stress distribution of the flame tube body is very uniform, and the stress value is also significantly higher than the stress value of the static force field. The reason for this phenomenon is that the flame tube body is affected by the temperature field, which changes the physical properties of the material to a certain extent. The existence of the temperature field increases the thermal stress of the flame tube itself, so that the stress of the flame tube itself is clearly greater than the stress in the static field. Obviously, it can be seen that the temperature field affects the internal molecular motion state of 316 L stainless steel, and when the multifield coupling is superimposed, the material stress is more obvious.

Figures 25 and 26 are the equivalent strain cloud diagram of the flame tube in the uncoupled case and the equivalent strain cloud diagram of the flame tube in the coupled case. From these two cloud diagrams, the influence of the temperature field on the strain of the flame tube can be seen. In Figure 25, it can be seen that the strain distribution of the flame tube in the static field is uneven, and the strain on the tube section and the top of the head is larger, and this part of the region is similar to the region with greater stress. In Figure 26, the strain distribution of the flame tube is relatively uniform. Under the action of the temperature field, the strain of the flame tube has increased, and the strain values of each area are also relatively close. It can be seen that the temperature field has a great influence on the flame tube.

9. Structural Optimization and Thermal Efficiency Analysis of High-Efficiency Oil-Fired Submersible Hot Water Machine

The thermal efficiency of oil-fired hot water machines has always been one of the focuses of people's research. The level of thermal efficiency directly affects the performance of the hot water machine. People mainly use two ways to improve thermal efficiency. One is to make fuel burn more. Sufficient, the second is to reduce the exhaust heat temperature of the flue gas by designing a reasonable structure. The fuel can be
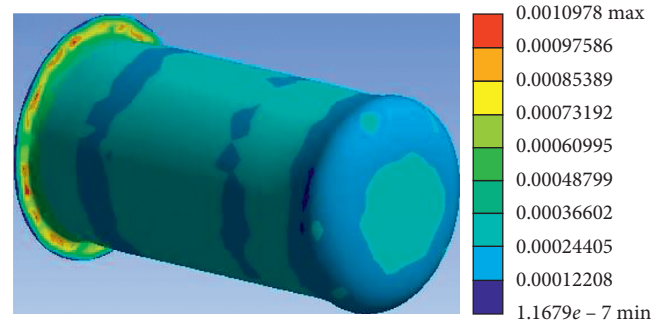
burned more fully by designing a reasonable combustion method.

9.1. Thermal Field Analysis of the Threaded Pipe. The factor of air supply is very important to whether the combustion reaction is sufficient. For this reason, it is necessary to establish the relationship between the change of the burner over time and the amount of air required. In Section 2.2, the theoretical air volume $V^0 = 11.153276 \, \mathrm{m^3/kg}$ has been calculated. The so-called theoretical air volume is the volume of air required when 1 kg of fuel is completely burned.

At time x, when y kg of 0# diesel is completely burned, the amount of air consumed is shown as follows:

$$\mathrm{d}U = 11.153276 \mathrm{d}x \mathrm{d}y. \tag{32}$$

Integrating equation (32), we can get

$$U = \iint_D \mathrm{d}U = \iint_D 11.153276 \mathrm{d}x \mathrm{d}y = 11.153276xy, \tag{33}$$

where definition domain $D = \{(x, y) | x \geq 0, y \geq 0\}$, D is the consumption of 0# diesel oil, kg.

The actual amount of gas produced by the hot water machine can be obtained through experiments. The relationship between the air supply volume and the thermal efficiency can be established by curve fitting through multiple sets of data.

9.2. Structural Optimization Model and Solution of Hot Water Machine. The parameters of the threaded pipe are thread radius (radius is divided into outer diameter, middle diameter, and inner diameter), length, wall thickness, pitch, arc radius, and thread groove depth. In order to ensure that the overall structure of the hot water machine does not undergo major changes, in the structural parameters of the threaded tube, the outer diameter of the threaded tube is limited to ensure that the structural parameters of the smoke chamber do not change. The relationship between the other parameters of the threaded tube and the thermal efficiency is now studied. By establishing the mathematical model of the relationship between the threaded tube of the hot water machine and the thermal efficiency, the influence of the threaded tube on the thermal efficiency is obtained.

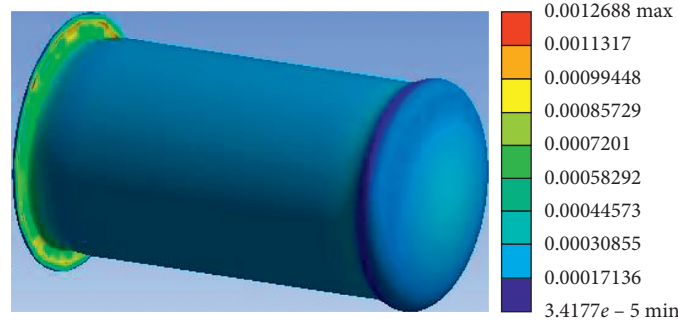The Newtonian cooling formula is shown as follows:

FIGURE 26: Equivalent strain cloud diagram of the coupled flame tube.

$$\Phi = hA\left(T_w - T_f\right), \tag{34}$$

where Φ is the convection heat transfer, W; h is the convection heat transfer coefficient, W/(m²·K); A is the heating surface area, m²; T_w is the temperature of the fire tube wall surface, °C; and T_f is the working fluid temperature, °C.

The general relationship of the convective heat transfer coefficient is shown as follows:

$$A = N\left[L_1 \pi d + L_2/s \cdot \sqrt{(\pi d_1)^2 + s^2} \cdot \left(\frac{ar\cos\left(\sqrt{r'^2 - (r' - t')^2}/r'\right)}{\pi} 2\pi r' - 2\sqrt{r'^2 - (r' - t')^2}\right)\right]. \tag{36}$$

where N is the number of threaded pipes, $N = 16$; L_1 is the total length of the threaded pipe, $L_1 = 0.71$ m; L_2 is the thread length of the threaded pipe, m; d is the outer diameter of the threaded pipe, $d = 0.032$ m; d_1 is the inner diameter of the threaded pipe, m; s is the thread pitch of the threaded pipe, m; t' is the inner diameter of the thread groove, m; and r' is the arc radius of the threaded pipe, m.

When burning 1 kg of 0# diesel, the heat absorbed by the working fluid water through convection heat transfer is shown as follows:

$$f(X) = -\lambda \frac{\partial T}{\partial y}\Big|_{y=0} \frac{1.14x_3 + 32x_1 \cdot \sqrt{(\pi x_2)^2 + x_3^2} \cdot \left(x_4 ar\cos\left(\sqrt{x_4^2 - (x_4 - x_5)^2}/x_4\right) - \sqrt{x_4^2 - (x_4 - x_5)^2}\right)}{42900x_3}. \tag{38}$$

The design variables are shown as follows:

$$X = [x_1, x_2, x_3, x_4, x_5]^T, \tag{39}$$

where x_1 is the thread length of the threaded pipe, m; x_2 is the inner diameter of the threaded pipe, m; x_3 is the thread pitch of the threaded pipe, m; x_4 is the arc radius of the threaded pipe, m; and x_5 is the thread groove depth, m.

9.2.2. Constraints. The constraint condition is shown as follows:

$$h = \frac{-\lambda \partial T/\partial y|_{y=0}}{T_w - T_f}, \tag{35}$$

where λ is the thermal conductivity of the working fluid water, $\lambda = 7.42 \times 10-2$, W/(m²·K), and $\partial T/\partial y|_{y=0}$ is the temperature change rate of the working fluid water in the normal direction of the fire tube wall, °C.

The area of the heating surface is shown as follows:

$$Q_{dl} = \int_T \Phi dt. \tag{37}$$

9.2.1. Objective Function. After substituting the corresponding values, the objective function of the ratio of the heat absorbed by the working fluid through the convection of the fire tube wall to the total heat transfer can be obtained as follows:

$$\begin{cases} 0 \le x_1 \le 0.700, \\ 0.028 \le x_2 \le 0.032, \\ x_3 > 0.010, \\ 0.005 \le x_5 \le 0.015, \\ 0 \le x_5 \le 0.004. \end{cases} \tag{40}$$

9.2.3. Optimization Methods and Results. The thermal efficiency structure model of the hot water machine is optimized by genetic algorithm. Genetic algorithm is an

$$(22.4 \text{ sqrt } (x^2 + (0.028 \ \pi)^2) \ (a \cos ((0.004 \ y - 0.002^2) \ /y)$$
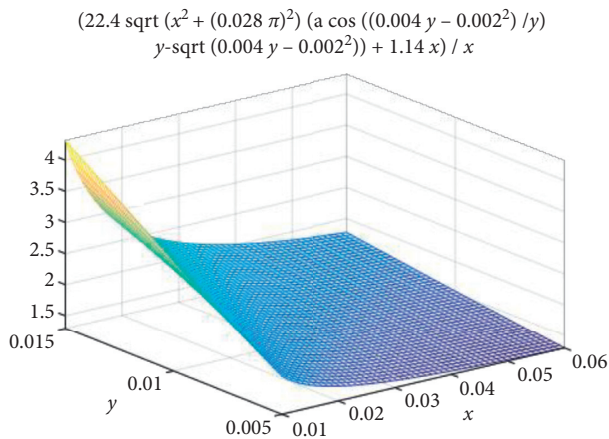$$y\text{-sqrt } (0.004 \ y - 0.002^2)) + 1.14 \ x) \ / \ x$$

Figure 27: Change of heated area of the threaded pipe.

algorithm that simulates the evolutionary laws of the biological world. By searching from random initial solutions, after a series of selection, crossover, and mutation steps, new ones are gradually calculated solution. The genetic algorithm can solve the structural optimization model of the thermal efficiency of the water heater better and faster, making the structural optimization of the water heater more accurate.

The MATLAB genetic algorithm optimizes the heating area of the threaded tube and draws the coordinate image with the pitch of the threaded tube and the radius of the arc as the independent variables. It can be seen from Figure 27 that when the thread pitch is 15 mm and the arc radius is 10 mm, the heated area of the threaded tube reaches the maximum.

10. Conclusion

The simulation results were compared with the theoretical calculation results, and the reliability of the simulation and the rationality of the structure design were obtained. The fluent software was used to simulate the thermal field of the flame tube and the threaded tube, and the rationality and accuracy of the thermal field of the flame tube and the threaded tube were obtained.

(1) The influence of the thermal structure coupling of the flame tube of the oil-fired submersible hot water machine was analyzed and studied. The total deformation cloud image, equivalent stress cloud image, and equivalent strain cloud image obtained by the thermal structure coupling results were compared with the corresponding cloud image under the action of the static force field. The influence of the temperature field on the flame tube of the oil-fired submersible hot water machine was explored.

(2) The thermal efficiency of the oil-fired submersible hot water machine was studied, the air supply model of the burner and the thread convection heat transfer model were established, and the genetic algorithm was optimized for the established model.

This article was to study the process of material compression molding and took out the part that involved heat separately for more comprehensive and in-depth research, so as to gain more experience and ideas [22].

Data Availability

The data used to support the findings of this study are included within the article.

Conflicts of Interest

The authors declare that they have no conflicts of interest.

Acknowledgments

References

[1] S. S. Rashwan, A. H. Ibrahim, T. W. Abou-Arab, M. A. Nemitallah, and M. A. Habib, "Experimental study of atmospheric partially premixed oxy-combustion flames anchored over a perforated plate burner," *Energy*, vol. 122, pp. 159–167, 2017.

[2] E. M. Wanjiru, S. M. Sichilalu, and X. Xia, "Optimal operation of integrated heat pump-instant water heaters with renewable energy," *Energy Procedia*, vol. 105, pp. 2151–2156, 2017.

[3] A. Yurtsev and G. P. Jenkins, "Cost-effectiveness analysis of alternative water heater systems operating with unreliable water supplies," *Renewable and Sustainable Energy Reviews*, vol. 54, pp. 174–183, 2016.

[4] H. Upadhye, R. Domitrovic, and A. Amarnath, "Using locational marginal pricing to implement peak load shifting with a grid connected water heater," *Ashrae Transactions*, 2013.

[5] K. Faloon, "Water heaters face 2015 mandate," *Supply House Times*, vol. 56, no. 9, pp. 36-37, 2013.

[6] G. Johnson and I. Beausoleil-Morrison, "The calibration and validation of a model for predicting the performance of gas-fired tankless water heaters in domestic hot water applications," *Applied Energy*, vol. 177, pp. 740–750, 2016.

[7] R. Lenhard and M. Malcho, "Numerical simulation device for the transport of geothermal heat with forced circulation of media," *Mathematical & Computer Modelling*, vol. 57, no. 1-2, pp. 111–125, 2013.

[8] Z. Liu, H. Li, K. Liu, H. Yu, and K. Cheng, "Design of high-performance water-in-glass evacuated tube solar water heaters by a high-throughput screening based on machine learning: a combined modeling and experimental study," *Solar Energy*, vol. 142, pp. 61–67, 2017.

[9] C. He, A. Giannis, and J.-Y. Wang, "Conversion of sewage sludge to clean solid fuel using hydrothermal carbonization: hydrochar fuel characteristics and combustion behavior," *Applied Energy*, vol. 111, pp. 257–266, 2013.

[10] J. Bujak and P. Sitarz, "Incineration of animal by-products—the impact of selected parameters on the flux of flue gas enthalpy," *Waste Management*, vol. 50, pp. 309–323, 2016.

[11] M. Qu, O. Abdelaziz, and H. Yin, "New configurations of a heat recovery absorption heat pump integrated with a natural

gas boiler for boiler efficiency improvement," *Energy Conversion and Management*, vol. 87, pp. 175–184, 2014.

[12] GB/T10180-2003, "Industrial boiler energy efficiency test and evaluation rules," *China Quality and Technical Supervision*, no. 12, pp. 20–23, 2010.

[13] H. Wang and L. Meng, "Present situation and direction of development of model WNS oil/gas fired boiler technology," *Journal of Engineering for Thermal Energy and Power*, no. 2, pp. 115–118 + 212, 2002.

[14] H. Huang, Z. Wu, G. Li, and J. Tan, "Improved design of an oil-fired hot-water boiler and its analysis," *Journal of Engineering for Thermal Energy and Power*, no. 5, pp. 461–464 + 543, 2006.

[15] M. Souliotis, S. Papaefthimiou, Y. G. Caouris, A. Zacharopoulos, P. Quinlan, and M. Smyth, "Integrated collector storage solar water heater under partial vacuum," *Energy*, vol. 139, pp. 991–1002, 2017.

[16] A. Hossain and Y. Nakamura, "Thermal and chemical structures formed in the micro burner of miniaturized hydrogen-air jet flames," *Proceedings of the Combustion Institute*, vol. 35, no. 3, pp. 3413–3420, 2015.

[17] F. Song, Z. Wen, Z. Dong, E. Wang, and X. Liu, "Ultra-low calorific gas combustion in a gradually-varied porous burner with annular heat recirculation," *Energy*, vol. 119, pp. 497–503, 2017.

[18] L. Dong, Y. Suzuki, and N. Kobayashi, "Experimental study on the performance of a hybrid water heater," *International Journal of Chemical Reactor Engineering*, vol. 7, no. 1, 2009.

[19] K. Tanha, A. S. Fung, and R. Kumar, "Performance of two domestic solar water heaters with drain water heat recovery units: simulation and experimental investigation," *Applied Thermal Engineering*, vol. 90, pp. 444–459, 2015.

[20] R. Manimaran and R. Senthilkumar, "Performance analysis of solar water heater at possible flow rates with and without phase change material," *Distributed Generation & Alternative Energy Journal*, vol. 31, no. 1, 2015.

[21] S. Pudaruth, J. T. Devi, and U. Y. Koodruth, "Understanding the ecological adoption of solar water heaters among customers of island economies," *Studies in Business & Economics*, vol. 12, no. 1, 2017.

[22] Y. Wang, Z. Zhu, L. Tang, and Q. Jiang, "Research on the molding design and optimization of the molding process parameters of the automobile trunk trim panel," *Advances in Materials Science and Engineering*, vol. 2020, Article ID 5629717, 19 pages, 2020.